NASA TECHNICAL NOTE

NASA TN D-4901

RESOLUTION CHANGES IN LITHIUM-DRIFTED SILICON SEMICONDUCTOR DETECTORS IRRADIATED WITH 0.5, 1.0, 2.0, AND 3.0 MeV ELECTRONS

by Herbert D. Hendricks and Donald H. Phillips

Langley Research Center
Langley Station, Hampton, Va.

NATIONAL AERONAUTICS AND SPACE ADMINISTRATION • WASHINGTON, D. C. • NOVEMBER 1968

RESOLUTION CHANGES IN LITHIUM-DRIFTED SILICON SEMICONDUCTOR DETECTORS IRRADIATED WITH 0.5, 1.0, 2.0, AND 3.0 MeV ELECTRONS

By Herbert D. Hendricks and Donald H. Phillips

Langley Research Center
Langley Station, Hampton, Va.

NATIONAL AERONAUTICS AND SPACE ADMINISTRATION

For sale by the Clearinghouse for Federal Scientific and Technical Information
Springfield, Virginia 22151 – CFSTI price $3.00

RESOLUTION CHANGES IN LITHIUM-DRIFTED SILICON SEMICONDUCTOR DETECTORS IRRADIATED WITH 0.5, 1.0, 2.0, AND 3.0 MeV ELECTRONS

By Herbert D. Hendricks and Donald H. Phillips
Langley Research Center

SUMMARY

Lithium-drifted silicon semiconductor detectors (2 mm deep and 80 mm^2 surface area) were irradiated with 0.5, 1.0, 2.0, and 3.0 MeV electrons. Fluence thresholds for damage were measured by monitoring resolution changes in the 0.972 MeV conversion electrons from ^{207}Bi. The fluence for 100-percent change in detector resolution was found to be approximately 10^{12} e/cm^2. Irradiations with 1 MeV electrons made at 10^7, 10^8, and 10^9 e/cm^2-sec gave no apparent flux dependence in the damage effects.

INTRODUCTION

In recent years semiconductor radiation detectors have taken over many of the spectrometer duties formerly undertaken with scintillation detectors and coincidence techniques. (See refs. 1 to 6.) These relatively new devices have given particle physicists a detector which has higher resolution, lower inherent background characteristics, higher efficiency, lower voltage requirements, and small size (refs. 4 and 5). The semiconductor detectors fall into three main types: surface barrier, diffused junction, and lithium-drifted detectors (ref. 5). All these detectors find use in nuclear physics laboratories, high- and low-energy accelerator laboratories, as well as in applications concerning the mapping of the Van Allen radiation belts and the space radiation environment in general. (See refs. 4, 7, 8, and 9.) Even with the advantages of the semiconductor detectors mentioned, there are disadvantages. These disadvantages are mainly resolution variations and radiation damage. (See ref. 10.) The resolution variation can be controlled by maintaining the detector at a fixed temperature. However, since the semiconductor detectors are used for counting the particles emitted from various radiation sources, there is an inherent degradation in resolution due to radiation damage. In order to determine the useful lifetime of the semiconductor detectors when used as a particle spectrometer, the determination of resolution as a function of the fluence was necessary. The resolution of the detector (designated FWHM (full width at half maximum), keV) is a measure of the detector's ability to distinguish between two adjacent electron energies. Resolution deterioration is a function of radiation type as well as semiconductor detector

type. The object of the study reported in this paper is to determine the effects of electron irradiation on the resolution of lithium-drifted silicon semiconductor detectors. The results of the effects of electron energies, electron flux, detector temperatures, and electron fluence are presented for lithium-drifted silicon semiconductor detectors.

APPARATUS AND TESTS

Accelerator

The semiconductor detectors were irradiated with electrons from a 1 MeV cascaded rectifier constant-potential-drop accelerator (ref. 11) and a 4 MeV Van de Graaff electrostatic accelerator (ref. 12). (1 MeV = 1.6×10^{-13} joules.) Electrons with incident kinetic energies over the range from 0.5 MeV to 3.0 MeV were used during the irradiations. The energy of the electrons from the accelerators was calibrated and monitored by using deep-depletion lithium-drifted semiconductor detectors and the radioactive isotope ^{207}Bi as a standard. Electrons stopped in the detectors give an output which is amplified and displayed on a multichannel analyzer. (This technique is discussed in further detail in the section "Electronic System.") By this calibration technique, the electron energy output from the accelerators can be determined. The electron-energy calibration of the accelerators was further confirmed by the use of energy-analyzing magnets. In the case of the Van de Graaff accelerator, the high-voltage calibration was also confirmed in the proton mode by using the proton-neutron threshold of a ^{6}Li target. The energy calibration determined by these methods agreed within ±4 keV. Energy stability of both accelerators also fell within the ±4 keV value.

Beam Handling System

Electrons from either accelerator were passed through an evacuated drift tube into a beam switching magnet. (See fig. 1.) The electrons were then bent through an angle and passed through a set of steering and quadrupole focusing magnets. The beam then traveled through a drift tube and impinged upon a scattering foil in the test chamber.

Test Chamber

The test chamber setup is shown in figures 1 and 2. The electron beam from the transport system was limited by a 0.635-cm-diameter aperture just prior to impinging upon a 0.0025-cm aluminum foil just inside the test chamber. The purposes of the foil were to scatter the electron beam and to spread the beam in order to obtain the lower electron flux. (See ref. 13.) An aluminum baffle thick enough to stop scattered electrons was placed near the center of the chamber. A hole in the center of the baffle allowed electrons to strike a beam-monitor aperture. The beam-monitor aperture had a 1.27-cm-diameter hole in the center in order to allow electrons through to irradiate the detector.

The beam-monitor aperture was insulated from ground and was used to monitor the electron beam during detector irradiations. Beam location and uniformity were determined by observing and measuring the darkening of polyvinylchloride film and cobalt glass. A Faraday cup on a rotating shaft was the primary electron beam monitor. The Faraday cup could be rotated in front of the detector housing aperture for electron flux determinations and then moved to one side during irradiations. A ^{207}Bi radioactive source was also mounted on a rotating shaft so it too could be positioned in front of the semiconductor detector aperture for checking the detector response. The test chamber was evacuated to a pressure of less than 2.2×10^{-4} N/m^2 during all tests. Various electrical feedthroughs were mounted on the chamber for detector bias and signal outputs as well as for power inputs to the thermoelectric cooler.

Test Samples and Sample Mounting

The semiconductor detectors used in this series of tests were commercially available lithium-drifted silicon detectors. (See refs. 14 and 15.) The detectors had the characteristics listed in table I. The depletion depth was 2 mm and corresponds approximately to the range of 1.2 MeV electrons in silicon. The detectors were mounted within an enclosed housing (figs. 2(c) and 2(d)) which had an 80-mm^2 circular entrance aperture. The detectors were attached to a thermoelectric cooler which was inside the detector housing. (See fig. 2(c).) The temperature of the detector case was monitored during test runs and maintained within $\pm 1^{\circ}$ C during testing. A check of detector face temperature and case temperature showed that no significant ($< 1^{\circ}$ C) temperature gradient was present after 1 hour of cooling.

Prior to the irradiations, each detector was measured for noise and leakage current as a function of temperature and bias voltage. A nominal bias voltage of 100 volts was chosen as an optimum value for minimum detector noise and leakage current over the temperature range of the test sequence. A value of 100 volts bias was sufficient to deplete the detector.

Electronic System

The electronic system (refs. 1, 4, and 16) used for this study is shown in block diagram form in figure 3. Part of the system consists of a charge-sensitive preamplifier (1-megohm bias resistor) and a linear amplifier. The output of the linear amplifier is processed by the multichannel analyzer and then read out into data storage systems. The amplifier system has a fixed 1-microsecond time constant in the integration and two differentiation stages. The amplifier system was operated in the resistance-capacitance (RC) mode. The average RC mode resolution due to amplifier noise was determined during tests with the aid of the multichannel analyzer. Tests with this system and a standard mercury pulser gave an average noise resolution of 5.4 keV and with a deviation

during tests of no greater than -1 or +2 keV. The resolution (ability to resolve two different adjacent electron energies) of the detectors was calculated (ref. 17) by subtracting the RC mode resolution due to amplifier noise.

A stabilized dc power supply was used to supply bias to the detector. The power supply included a current meter for leakage current measurements. An oscilloscope was attached at the amplifier output to detect amplifier saturation and operation conditions. A root-mean-square voltmeter was also connected at this point to measure detector root mean square noise and to check for microplasma breakdown (internal electric field breakdown in semiconductor detectors). The detectors were mounted on a thermoelectric cooler the temperature of which was kept constant to within $\pm 1^{\circ}$ C by a thermoregulator which controlled the power supply to the cooler. A thermocouple was used to monitor the detector case temperature.

The multichannel analyzer input amplifier discriminator was set so that the zero channel was equivalent to approximately 50 keV electrons. However, this value was confirmed and a calibration curve of the type shown in figure 4 was determined for each detector. The solid line curve in figure 4 represents a plot of counts as a function of channel number (right ordinate) and is a typical spectrum output from the multichannel analyzer. The calibration curve (straight line) of energy in MeV (left ordinate) as a function of channel number was obtained by using the known internal conversion electron energy from the standard radioactive source ^{207}Bi. An accelerator calibration spectrum such as shown in figure 4 (dashed line) for 0.5 MeV and 1 MeV was obtained by counting particles from the accelerators and displaying the output in such a fashion as shown. Shown at the right of this curve are the mercury pulser peaks (previously discussed) for determining resistance-capacitance mode noise resolution.

The overall electronic system calibration and the resolution for any number of electron energies could be obtained from curves of the type shown in figure 4. In actual practice, the data from the multichannel analyzer were read out onto an X,Y recorder, a typewriter, and stored for permanent record on punched tape. The actual energy calibration and resolution were calculated from the typed data and applied to the recorder plots. The overall system stability as measured by a mercury pulser for each test sequence was better than ± 2 keV.

Test Procedures

The lithium-drifted detectors were mounted in the test chamber as shown in figures 1 and 2. A pressure of less than 2.2×10^{-4} N/m^2 was obtained within the test chamber before proceeding with any test. After obtaining this pressure the thermoelectric cooler was set to give one of the three temperatures listed in table II, namely, 0°, 10°, or 20° C. After a particular temperature was established, a calibration curve of the type

shown in figure 4 was obtained. The ^{207}Bi spectrum was obtained by rotating the radioactive source in front of the detector housing aperture. The conversion electrons from the source impinge upon the semiconductor detector where the electrons are absorbed. The detector and electronics system (fig. 3) amplify and display (fig. 4) the energy-intensity distribution of the electrons stopped within the detector. The gain and noise of the overall system were measured by using a mercury pulser as a reference. When the output from the mercury pulser was repeated at the same pulse height level of the multichannel analyzer and was maintained at approximately the same resistance-capacitance mode noise resolution, the system was judged to be stable and suitable for continuing tests. As previously described, the calibration curve (fig. 4) of electron energy as a function of channel number was obtained from the output of the multichannel analyzer.

Prior to each incremental fluence for each set of conditions shown in table II, information giving the type of calibration curves shown in figure 4 was collected. The information was then stored on punched tape, typed out, and traced by an X,Y recorder. The increments in which each detector was exposed to electron radiation are given in tables III to VI. A standard calculation (ref. 17) in which the electronics system noise contribution is subtracted was used to obtain the resolution data. The detector temperature was controlled to within less than $\pm 1^{o}$ C of the test conditions given in table II. The noise level and leakage current of each detector were monitored before, during, and after each test. Permanent changes of noise level and leakage current were insignificant (< 5 percent) and were not tabulated.

Prior to each irradiation, the accelerator was turned on and set to the electron energy for one of the sets of test conditions given in table II. The beam current was set by using the Faraday cup and beam monitor aperture shown in figures 1 and 2. After establishing the correct flux (table II), the beam was stopped from going into the test chamber by closing a gate valve. The Faraday cup which had been initially in front of the detector housing aperture was removed to one side. The beam monitor aperture was connected to an integrating electrometer. The incremental fluence to be recorded by this integrating electrometer was determined previously by calibration of the Faraday cup with the beam monitor aperture currents. To start the exposure, the gate valve was opened and the integrating electrometers started. Once the correct exposure dose had been obtained, the valve was closed and the accelerator turned off. The information necessary to obtain the data presented in tables III to VI as well as figures 5 to 8 was then obtained by collecting a ^{207}Bi spectrum (fig. 4). The live time accumulation used to obtain each ^{207}Bi spectrum on the multichannel analyzer was 20 minutes. This procedure was continued until a change of at least 100 percent in the resolution of the detector was obtained (referenced to the 0.972 MeV conversion electron from ^{207}Bi).

RESULTS AND DISCUSSION

Resolution changes in lithium-drifted semiconductor detectors were studied as a function of exposed electron fluence for several electron energies. The detectors studied have the characteristics given in table I. The various experimental parameters varied during these tests are given in table II. As previously discussed, a ^{207}Bi conversion electron spectrum of the type shown in figure 4 was the main data collected. The 0.972 MeV conversion electrons from the ^{207}Bi source were the standard for comparison of resolution changes during all tests. A typical degradation sequence is shown in figure 9 only for the 0.972 MeV conversion electron from the ^{207}Bi radioactive source.

For the unirradiated case the semiconductor detector gave a calibration curve with the electron energy peak equal to 0.972 MeV and a given resolution. The resolution of the detector (FWHM (full width at half maximum), keV) is a measure of the detector's ability to distinguish between two adjacent electron energies. In the case cited in figure 9, the resolution is 22 keV.

From figure 9, it is to be noted that as the detectors are irradiated with electrons, a degradation process takes place. This process is seen mainly by a shift in the peak electron energy (a change in energy calibration) and a change in resolution (ability to resolve two discrete electrons of different energies). The following discussion is centered about the threshold electron fluence for energy calibration change and that fluence for 100-percent change in detector resolution. It is to be noted that more electron fluence is required for degradation of the detectors at 0.5 MeV than at higher electron energies. A low-energy electron is scattered easily and thus loses energy rapidly. This energy loss subsequently lowers the initial electron energy below a threshold at which defect production takes place. Therefore, more low-energy electrons are required than high-energy electrons to produce the same effect.

0.5 MeV Irradiations

Figure 5 shows the changes in resolution of four detectors, irradiated with 0.5 MeV electrons, as a function of fluence. The threshold accumulated fluence at which the energy calibration begins to change as well as the resolution begins to deteriorate is approximately 10^{13} e/cm^2. The accumulated fluence in which the detector resolution has changed 100 percent is approximately 2×10^{13} to 3×10^{13} e/cm^2, that is, the fluence that doubles original increment between two barely distinguishable adjacent energies. The actual data concerning the resolution values are given in table III. By studying this table, it is to be noted that there is a process in which the resolution recovers after each incremental fluence but does not recover to the previous value. This recovery process (ref. 18) was noted as a function of time (table III) after irradiation. No smooth predictable trend toward the final recovery was noted. However, nearly all the detectors showed a recovery of resolution after some stage of irradiation.

1.0 MeV Irradiations

Figure 6 shows the changes in resolution of nine detectors, irradiated with 1.0 MeV electrons, as a function of fluence. The threshold accumulated fluence at which the energy calibration begins to change as well as the resolution begins to deteriorate is approximately 0.3×10^{12} to 0.7×10^{12} e/cm^2. The accumulated fluence in which the detector resolution has changed 100 percent is approximately 0.8×10^{12} to 1.2×10^{12} e/cm^2. The actual data concerning the resolution values are given in table IV. The comments concerning recovery time of the detector resolution are the same as those for the 0.5 MeV irradiations.

2.0 MeV Irradiations

Figure 7 shows the changes in resolution of five detectors, irradiated with 2.0 MeV electrons, as a function of fluence. The threshold accumulated fluence at which the energy calibration begins to change as well as the resolution begins to deteriorate is approximately 0.2×10^{12} to 0.5×10^{12} e/cm^2. The accumulated fluence in which the detector resolution has changed 100 percent is approximately 0.3×10^{12} to 0.8×10^{12} e/cm^2. The actual data concerning the resolution values are given in table V. The comments concerning recovery of the detector resolution recovery are the same as those for the 0.5 MeV irradiations.

3.0 MeV Irradiations

Figure 8 shows the changes in resolution of three detectors, irradiated with 3.0 MeV electrons, as a function of fluence. The threshold accumulated fluence at which the energy calibration begins to change as well as the resolution begins to deteriorate is approximately 0.4×10^{12} to 0.7×10^{12} e/cm^2. The accumulated fluence in which the detector resolution has changed 100 percent is approximately 0.5×10^{12} to 0.8×10^{12} e/cm^2. The actual data concerning the resolution values are given in table VI. The comments concerning recovery of the detector resolution recovery are the same as those for the 0.5 MeV irradiations.

General Test Results

The overall threshold for damage to the lithium-drifted semiconductor detectors studied in this series of tests lies between 0.2×10^{12} and 10^{13} e/cm^2 (table VII). This threshold range for damage by 0.5 to 3.0 MeV electrons is applicable to the situation where the detectors are used as electron spectrometers. However, the detectors are still useful for counting and detecting particles.

The leakage current and noise level of the detectors were monitored for all series of the tests. However, no significant changes (> 5 percent) were noted during any of the tests.

In the cases (tables IV(a) and IV(b)) where the electron flux was varied, there appeared to be no significant flux dependence concerning damage effects monitored during this series of tests. This result may be noted mainly by studying the 1 MeV test data shown in figure 6 and tables IV(a) and IV(b).

Figure 10 shows one of the cases where multiple peaking (refs. 5 and 17 discuss cases for heavy particles) of the 0.972 MeV ^{207}Bi conversion electron peaks was observed during the test sequence. This particular feature was recorded on three different detectors (one each at 1, 2, and 3 MeV) of the 900 ohm-cm base silicon. In each case the multiple peaking was checked to determine whether there would be a merging of the peaks during the "recovery" process. During this period the detectors were monitored for approximately 16 hours and the peaks did not merge. These three occurrences were noted after an exposure of 0.5×10^{12} to 0.7×10^{12} e/cm^2. The multiple peaking disappeared after the next incremental electron fluence was given to the detectors.

CONCLUSIONS

The series of electron irradiation tests at 0.5, 1.0, 2.0, and 3.0 MeV on lithium-drifted semiconductor detectors points again to the need for more radiation-resistant semiconductor devices. The fluence at which deterioration of the detector begins is too low (without extensive collimination) for extended use as an electron spectrometer in the near-earth space radiation environment. The main conclusions to be drawn from the tests discussed are:

1. The overall threshold for damage to the detectors studied lies between 0.2×10^{12} and 10^{13} e/cm^2 (for electrons of energies between 0.5 and 3.0 MeV).

2. The overall fluence for 100-percent change in detector resolution is 0.3×10^{12} to 2×10^{13} e/cm^2 (for electrons of energies between 0.5 and 3.0 MeV).

3. There appeared to be no significant difference in damage threshold for a flux of 10^7, 10^8, 10^9 e/cm^2-sec for the 1 MeV irradiations.

Langley Research Center,
National Aeronautics and Space Administration,
Langley Station, Hampton, Va., July 24, 1968,
124-09-12-01-23.

REFERENCES

1. Goulding, Fred S.: Semiconductor Detectors – Their Properties and Applications. Nucleonics, vol. 22, no. 5, May 1964, pp. 54-61.

2. Glos, Margaret Beach: Semiconductors, Scintillators and Data Analysis. Nucleonics, vol. 22, no. 5, May 1964, pp. 50-72.

3. Miller, G. L.; Gibson, W. M.; and Donovan, P. F.: Semiconductor Particle Detectors. Annu. Rev. Nucl. Sci., vol. 12, Emilio Segrè Gerhart Friedlander, and Walter E. Meyerhof, eds., Annu. Reo., Inc., 1962, pp. 189-219.

4. Goulding, F. S.: Semiconductor Detectors for Nuclear Spectrometry, I. Nucl. Instr. Methods, vol. 43, no. 1, Aug. 1, 1966, pp. 1-54.

5. Dearnaley, G.; and Northrop, D. C.: Semiconductor Counters for Nuclear Radiations. Second ed., E. & F. N. Spon, Ltd. (London), 1966.

6. Taylor, J. M.: Semiconductor Particle Detectors. Butterworth Inc., c.1963.

7. McCormac, Billy M. ed.: Radiation Trapped in the Earth's Magnetic Field. Gordon and Breach Science Publ., Inc., 1966.

8. Vette, James I.: Models of the Trapped Radiation Environment. Volume I: Inner Zone Protons and Electrons. NASA SP-3024, 1966.

9. Bromley, D. A.: Semiconductor Detectors in Nuclear Physics. Semiconductor Nuclear Particle Detectors, J. W. T. Dabbs and F. J. Walter, eds., Publ. 871, Nat. Acad. Sci. – Nat. Res. Counc., 1961, pp. 61-73.

10. Dearnaley, Geoff: Radiation Damage Effects in Semiconductor Detectors. Nucleonics, vol. 22, no. 7, July 1964, pp. 78-85.

11. Cleland, M. R.; and Morganstern, K. H.: A New High-Power Electron Accelerator. IRE, Trans. Ind. Electron., vol. IE-7, no. 2, July 1960, pp. 36-40.

12. Livingston, M. Stanley; and Blewett, John P.: Particle Accelerators. McGraw-Hill Book Co., Inc., 1962, pp. 30-72.

13. Nablo, Sam V.; and Beggs, William C.: Simulation of the Near Terrestrial Space Radiation Environment. Test Eng. Manage., vol. 13, no. 2, Feb. 1965, pp. 55-62.

14. Ziemba, F. P.: Research and Development on Fabrication of Pin and Lid Detectors and the Dry Run Interface System. UCRL-13106 (AEC Contract No. W-7405-eng-48), Lawrence Radiat. Lab., Univ. of California, Aug. 31, 1963.

15. Miller, G. L.; Pate, B. D.; and Wagner, S.: Production of Thick Semiconductor Radiation Detectors by Lithium Drifting. IEEE Trans. Nucl. Sci., vol. NS-10, no. 1, Jan. 1963, pp. 220-229.

16. Mayer, J. W.: Pulse Formation in Semiconductor Detectors. Semiconductor Nuclear Particle Detectors, J. W. T. Dabbs and F. J. Walter, eds., Publ. 871, Nat. Acad. Sci. – Nat. Res. Counc., 1961, pp. 1-8.

17. Evans, Robley D.: The Atomic Nucleus. McGraw-Hill Book Co., Inc., c.1955.

18. George, G. G.; and Gunnersen, E. M.: Irradiation Damage Effects in Silicon Surface Barrier Counters. Nucl. Inst. Methods, vol. 25, no. 2, Jan. 1964, pp. 253-260.

TABLE I.- LITHIUM-DRIFTED SILICON SEMICONDUCTOR DETECTOR CHARACTERISTICS

Detector active area, mm^2	80
Depletion depth, mm	2
Minority carrier lifetime (of base silicon), μsec	1000
Resistivity (of base silicon), ohm-cm	750 and 900
Detector bias voltage, volts (nominal)	100

TABLE II.- TEST PARAMETERS OF SEMICONDUCTOR RADIATION DETECTORS EVALUATED

Detector serial numbers	Temperature, °C	Electron energy, MeV	Flux, e/cm^2-sec	Resistivity (base silicon), ohm-cm	Bias voltage, volts
742	0	0.5	10^9	900	100
861	10	.5	10^9	900	100
741	10	.5	10^9	900	100
749	20	.5	10^9	900	100
744	0	1.0	10^7	900	100
747	0	1.0	10^8	900	100
850	10	1.0	10^8	750	100
849	20	1.0	10^8	750	100
847	0	1.0	10^9	750	200
740	0	1.0	10^9	900	100
748	0	1.0	10^9	900	100
752	10	1.0	10^9	900	100
739	20	1.0	10^9	900	100
751	0	2.0	10^9	900	100
750	0	2.0	10^9	900	100
754	0	2.0	10^9	900	100
860	0	2.0	10^9	750	100
848	10	2.0	10^9	750	100
746	0	3.0	10^9	900	100
745	10	3.0	10^9	900	100
753	20	3.0	10^9	900	100

TABLE III.- SEMICONDUCTOR DETECTOR RESOLUTION CHANGES AS A FUNCTION OF FLUENCE OF 0.5 MeV ELECTRONS

Detector 742 for –		Detector 861 for –		Detector 741 for –		Detector 749 for –	
0^{o} C and 10^{9} e/cm^{2}-sec		10^{o} C and 10^{9} e/cm^{2}-sec		10^{o} C and 10^{9} e/cm^{2}-sec		20^{o} C and 10^{9} e/cm^{2}-sec	
Resolution, FWHM-keV	Fluence, e/cm^{2}	Resolution, FWHM-keV	Fluence, e/cm^{2}	Resolution, FWHM-keV	Fluence, e/cm^{2}	Resolution, FWHM-keV	Fluence, e/cm^{2}
20.8	0	27	0	24.4	0	27	0
20.7	10^{10}	24	10^{10}	24.1	10^{10}	26.6	10^{10}
21.5	10^{11}	24	10^{11}	23.4	10^{11}	27.4	10^{11}
20.4	5×10^{11}	26	10^{12}	23.3	10^{12}	26.5	10^{12}
21.4	6×10^{11}	34.5	10^{13}	25	4×10^{12}	27.4	10^{13}
22.0	7×10^{11}	33.3	1.1×10^{13}	24.5	1-hour recovery	31.6	1.2×10^{13}
22.2	8×10^{11}	26	16-hour recovery	32.4	10^{13}	29.1	16-hour recovery
21.1	9×10^{11}	35.7	2×10^{13}	43	2×10^{13}	44	2×10^{13}
20.9	10^{12}	47.4	3×10^{13}	37.1	1-hour recovery	39.6	1-hour recovery
20.9	1.1×10^{12}					46.25	2.8×10^{13}
21	16-hour recovery						
21.7	1.2×10^{12}						
21.4	1.3×10^{12}						
21	1.4×10^{12}						
21.4	1.5×10^{12}						
20.6	1.6×10^{12}						
31.2	10^{13}						
27	2-hour recovery						
45.1	2×10^{13}						
37.4	2-hour recovery						
37.5	1-hour recovery						

TABLE IV.- SEMICONDUCTOR DETECTOR RESOLUTION CHANGES AS A FUNCTION OF FLUENCE OF 1 MeV ELECTRONS

Detector 0744 for – 0° C and 10^7 e/cm^2-sec		Detector 747 for – 0° C and 10^8 e/cm^2-sec		Detector 850 for – 10° C and 10^8 e/cm^2-sec	
Resolution, FWHM-keV	Fluence, e/cm^2	Resolution, FWHM-keV	Fluence, e/cm^2	Resolution, FWHM-keV	Fluence, e/cm^2
22.5	0	20.3	0	35.9	0
20.3	1.13×10^8	22.1	6.4×10^8	37.1	10^9
21.5	1.13×10^9	23.3	6.4×10^9	40.9	10^{10}
19.7	1.13×10^{10}	22.8	6.4×10^{10}	36.9	5×10^{10}
20.6	5.65×10^{10}	34.9	6.4×10^{11}	36.5	10^{11}
18.8	1.13×10^{11}	184	1.93×10^{12}	41.3	2×10^{11}
19.54	2.3×10^{11}	*106*	*16-hour recovery*	42.2	3×10^{11}
20.6	3.4×10^{11}	173	2.6×10^{12}	48.4	4×10^{11}
31.3	4.5×10^{11}	181	3.2×10^{12}	46.7	5×10^{11}
65.7	5.6×10^{11}	172	2-hour recovery	47.6	6×10^{11}
55.2	*48-hour recovery*	216	3.8×10^{12}	49.6	7×10^{11}
64.4	6.8×10^{11}	189	1-hour recovery	59.4	8×10^{11}
90.4	7.9×10^{11}	221	4.5×10^{12}	84.5	9×10^{11}
90.2	16-hour recovery	179	1-hour recovery	82.8	10^{12}
				90.4	1.1×10^{12}
				92.0	1.2×10^{12}
				92.8	1.3×10^{12}

Detector 849 for – 20° C and 10^8 e/cm^2-sec		Detector 0847 for – 0° C and 10^9 e/cm^2-sec		Detector 0740 for – 0° C and 10^9 e/cm^2-sec	
Resolution, FWHM-keV	Fluence, e/cm^2	Resolution, FWHM-keV	Fluence, e/cm^2	Resolution, FWHM-keV	Fluence, e/cm^2
46.6	0	28.8	0	18.6	0
48	10^{11}	33.7	1.3×10^{10}	20.4	10^{10}
49	2×10^{11}	30.4	10^{11}	18.9	5×10^{10}
58	4×10^{11}	40.2	2.8×10^{11}	19	10^{11}
65.5	6×10^{11}	45.9	5×10^{11}	19.6	2×10^{11}
62.8	16-hour recovery	49.6	7×10^{11}	20.4	3×10^{11}
69.1	8×10^{11}	46.2	16-hour recovery	19.7	4×10^{11}
114.6	10^{12}	52.1	9×10^{11}	20.4	5×10^{11}
		62.9	1.1×10^{12}	26.6	6×10^{11}
		214	2×10^{12}	52.6	7×10^{11}
		138	48-hour recovery	33	16-hour recovery
				78.5	8×10^{11}
				116.8	9×10^{11}
				89	1-hour recovery
				79.7	2-hour recovery

Detector 748 for – 0° C and 10^9 e/cm^2-sec		Detector 752 for – 10° C and 10^9 e/cm^2-sec		Detector 739 for – 20° C and 10^9 e/cm^2-sec	
Resolution, FWHM-keV	Fluence, e/cm^2	Resolution, FWHM-keV	Fluence, e/cm^2	Resolution, FWHM-keV	Fluence, e/cm^2
18.5	0	23.4	0	28.8	0
18.3	10^{10}	22.9	10^{10}	28.5	10^{10}
18.2	5×10^{10}	22.3	10^{11}	26.3	5×10^{10}
18.2	10^{11}	21.6	5×10^{11}	26.4	10^{11}
18	2×10^{11}	24.4	6×10^{11}	27	2×10^{11}
17.6	3×10^{11}	36.1	7×10^{11}	27.6	3×10^{11}
18	4×10^{11}	64	8×10^{11}	27.9	4×10^{11}
21.7	5×10^{11}	109	9×10^{11}	28.6	5×10^{11}
43.6	6×10^{11}	79.2	10^{12}	29	6×10^{11}
81.8	7×10^{11}			37.7	7×10^{11}
66.8	8×10^{11}			76.7	8×10^{11}
50.5	3-hour recovery			77.2	9×10^{11}
76.1	9×10^{11}				

TABLE V.- SEMICONDUCTOR DETECTOR RESOLUTION CHANGES AS A FUNCTION OF FLUENCE OF 2.0 MeV ELECTRONS

Detector 751 for –		Detector 750 for –		Detector 754 for –		Detector 860 for –		Detector 848 for –	
0^{o} C and 10^{9} e/cm^{2}-sec		0^{o} C and 10^{9} e/cm^{2}-sec		0^{o} C and 10^{9} e/cm^{2}-sec		0^{o} C and 10^{9} e/cm^{2}-sec		10^{o} C and 10^{9} e/cm^{2}-sec	
Resolution, FWHM-keV	Fluence, e/cm^{2}	Resolution, FWHM-keV	Fluence, e/cm^{2}	Resolution, FWHM-keV	Fluence, e/cm^{2}	Resolution, FWHM-keV	Fluence, e/cm^{2}	Resolution, FWHM-keV	Resolution, FWHM-keV
16.1	0	16.4	0	19.7	0	23.8	0	22.5	0
16.4	10^{10}	15.5	10^{10}	18.3	10^{10}	24	10^{11}	23	10^{11}
16.6	10^{11}	17.5	10^{11}	20.8	10^{11}	28.2	2×10^{11}	27.8	2×10^{11}
19.6	2×10^{11}	19.5	4×10^{11}	19.4	2×10^{11}	118	4×10^{11}	100	4×10^{11}
66.28	4×10^{11}	34.5	6×10^{11}	27	4×10^{11}	110	6×10^{11}	65.4	1-hour recovery
33.3	16-hour recovery	59.3	8×10^{11}	168	6×10^{11}	80.7	16-hour recovery	82.5	6×10^{11}
50.3	5×10^{11}	152	10^{12}	61	1-hour recovery				
71	6×10^{11}			149	8×10^{11}				
61	16-hour recovery								
189	8×10^{11}								
64.6	1-hour recovery								
56.6	2-hour recovery								
140	10^{12}								
128	3-hour recovery								

TABLE VI.- SEMICONDUCTOR DETECTOR RESOLUTION CHANGES AS A FUNCTION FLUENCE OF 3.0 MeV ELECTRONS

Detector 746 for –		Detector 753 for –		Detector 745 for –	
0^{o} C and 10^{9} e/cm^2-sec		20^{o} C and 10^{9} e/cm^2-sec		10^{o} C and 10^{9} e/cm^2-sec	
Resolution, FWHM-keV	Fluence, e/cm^2	Resolution, FWHM-keV	Fluence, e/cm^2	Resolution, FWHM-keV	Fluence, e/cm^2
14	0	35	0	22.7	0
17.4	10^{10}	36.3	10^{11}	24.1	10^{11}
19.5	10^{11}	37.7	2×10^{11}	26.3	2×10^{11}
18.8	2×10^{11}	40.2	4×10^{11}	26.9	4×10^{11}
21.0	3×10^{11}	179	6×10^{11}	144	6×10^{11}
20.4	1-hour recovery	38.4	1-hour recovery	32.5	5-hour recovery
21.4	4×10^{11}	88.7	8×10^{11}	227	8.1×10^{11}
89.7	5×10^{11}	187	10^{12}	74.5	2-hour recovery
63.4	1-hour recovery			166	10^{12}
32.5	2-hour recovery				
57.7	6×10^{11}				
96.9	8×10^{11}				
78.8	3-hour recovery				
68.7	7-hour recovery				

TABLE VII.- SUMMARY OF THE RESULTS OF ACCUMULATED FLUENCE EFFECTS AT DIFFERENT ELECTRON ENERGIES

Electron energy, MeV	Threshold fluence, e/cm^2	Fluence for 100-percent resolution change, e/cm^2
0.5	10^{13}	2×10^{13} to 3×10^{13}
1.0	0.3×10^{12} to 0.7×10^{12}	0.8×10^{12} to 1.2×10^{12}
2.0	$.2 \times 10^{12}$ to 0.5×10^{12}	$.3 \times 10^{12}$ to 0.8×10^{12}
3.0	$.4 \times 10^{12}$ to 0.7×10^{12}	$.5 \times 10^{12}$ to 0.8×10^{12}

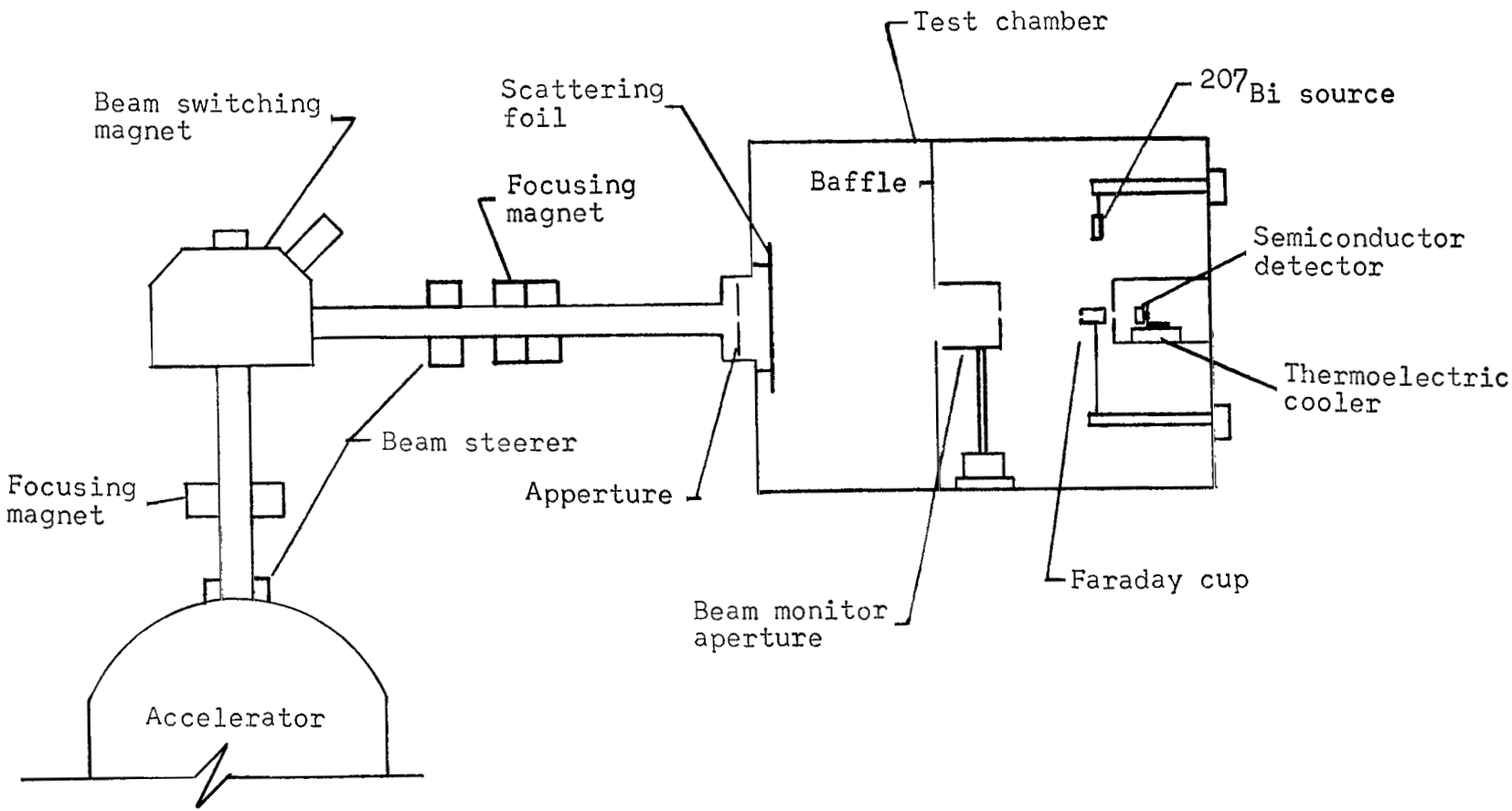

Figure 1.- Diagram of the accelerator, beam transport system, and test arrangement.

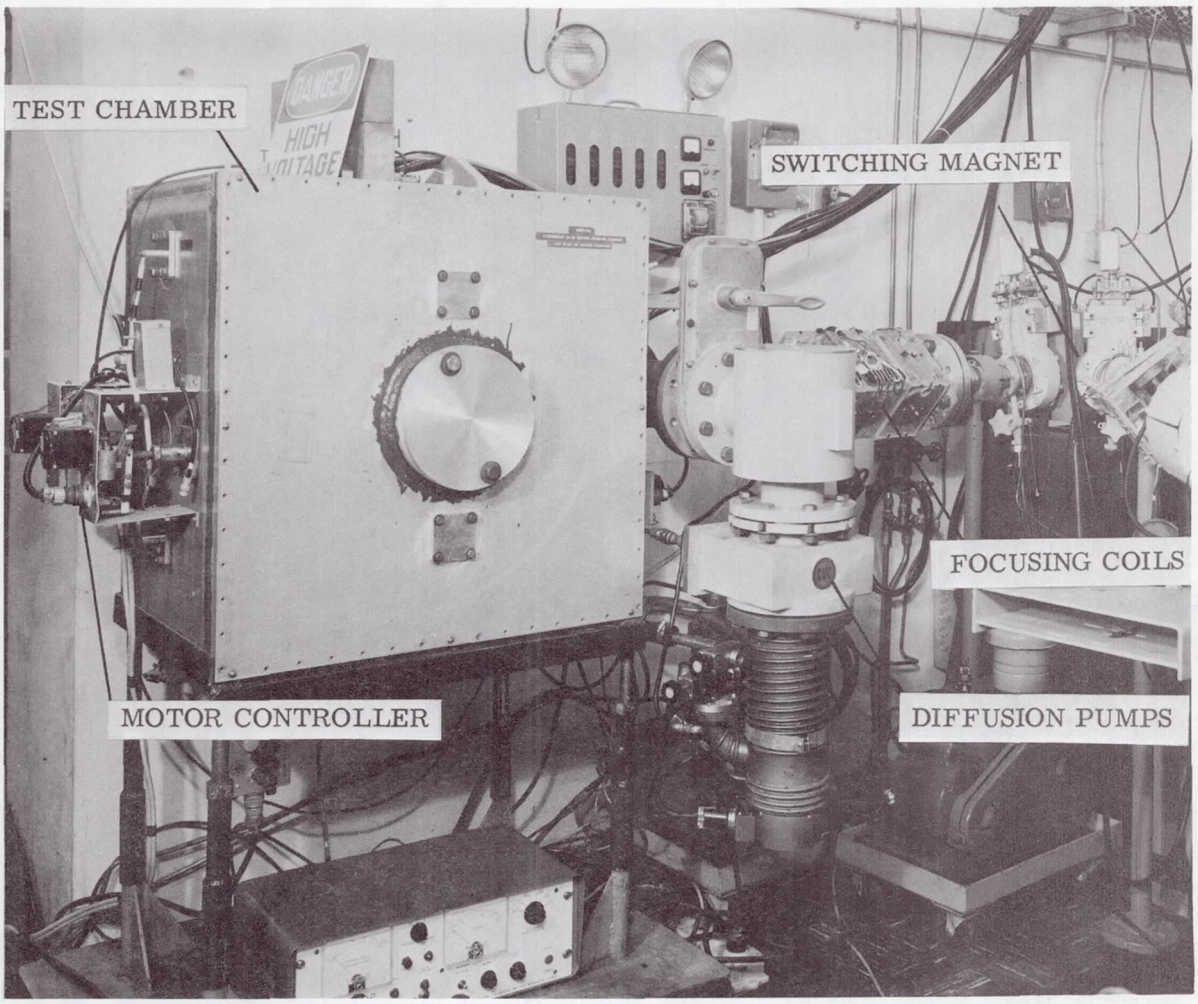

(a) Test chamber, vacuum system, and beam transport. L-67-1104.1

Figure 2.- Test chamber, beam transport system, and inside of test chamber showing detector test apparatus.

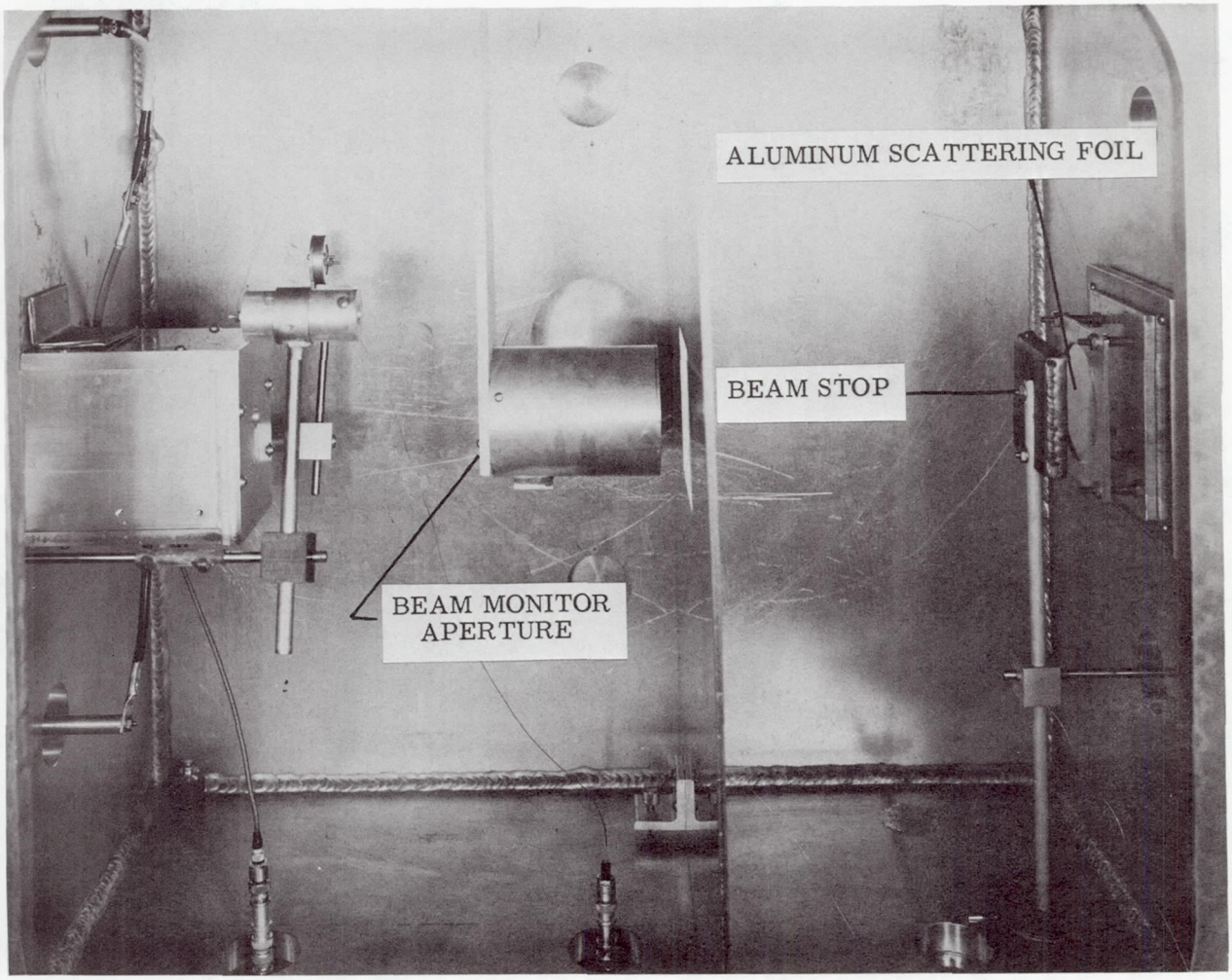

L-67-1103.1

(b) Inside of test chamber showing location of scattering foil, monitor aperture, and sample holder.

Figure 2.- Continued.

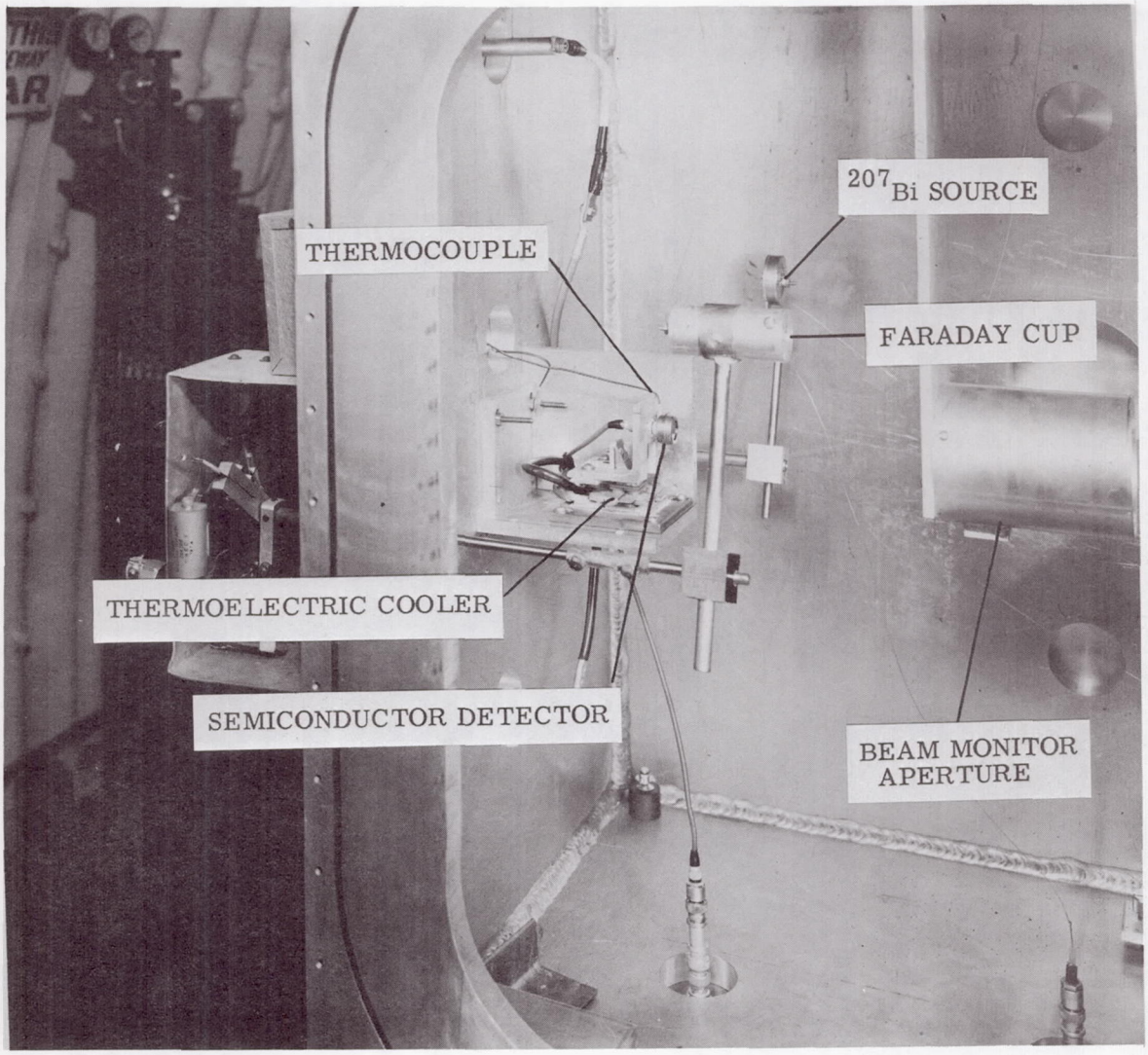

(c) Inside of test chamber showing part of cover removed from detector box and relation of test apparatus within box. L-67-1101.1

Figure 2.- Continued.

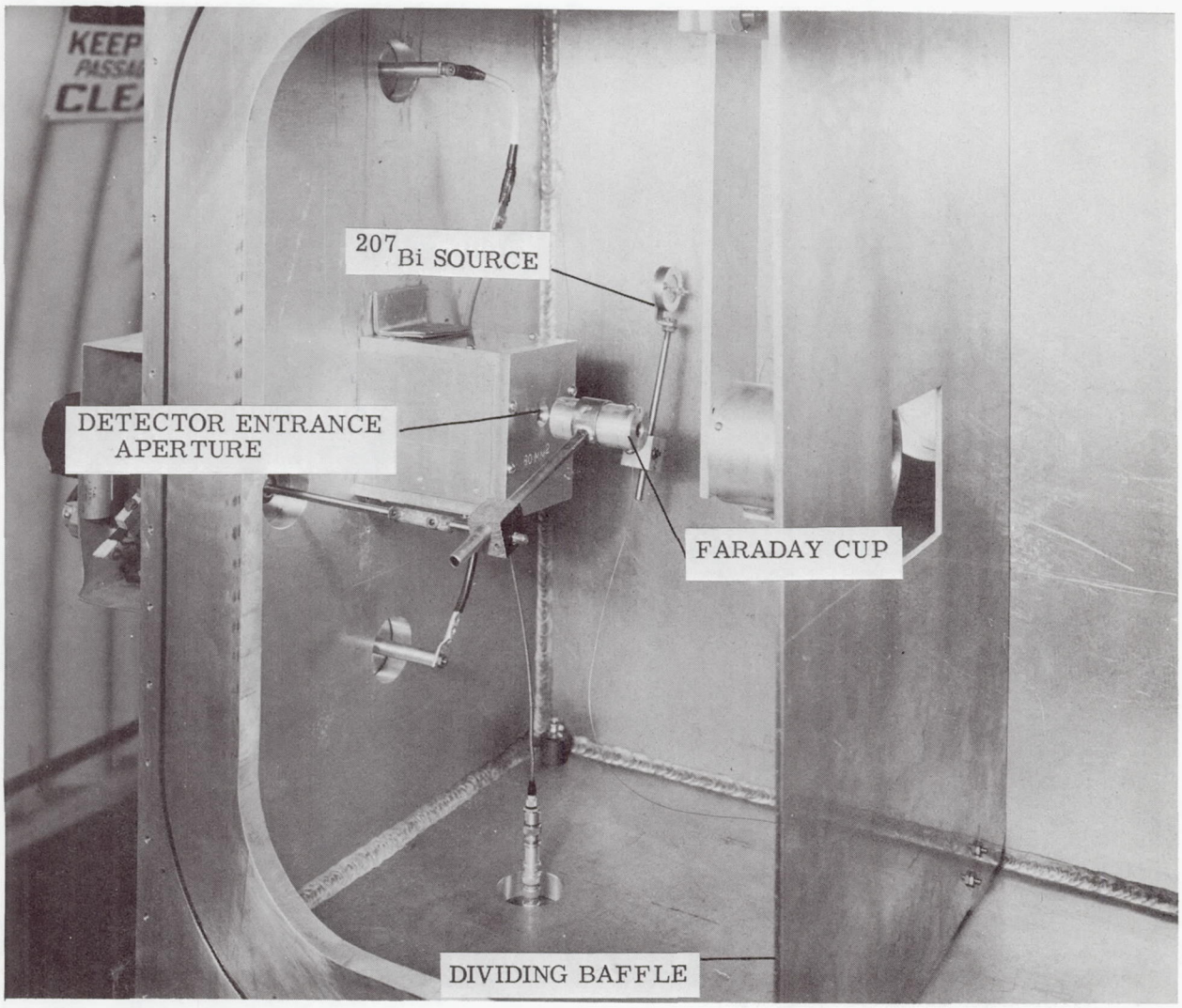

(d) Inside of test chamber showing location of Faraday cup and reference source in respect to detector entrance aperture. L-67-1106.1

Figure 2.- Concluded.

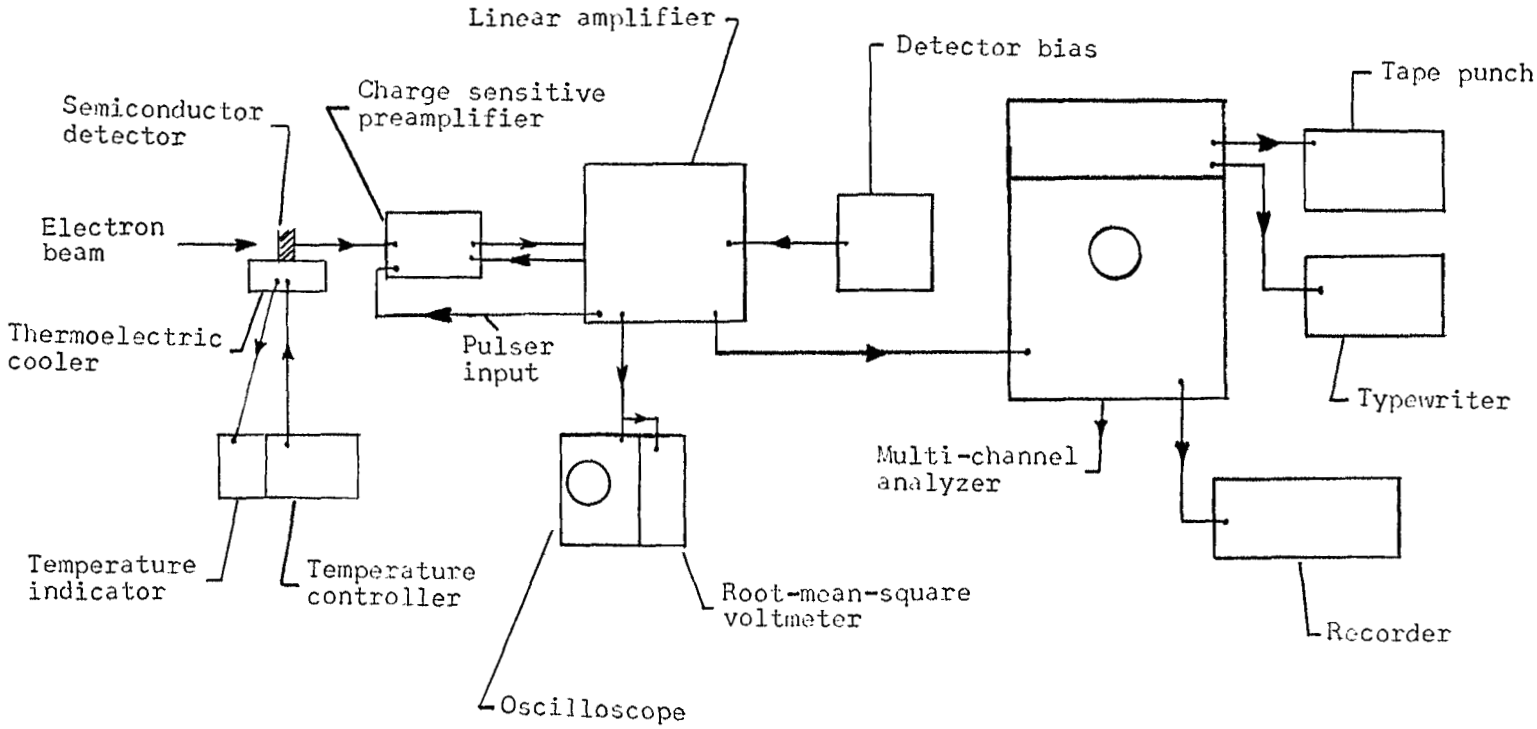

Figure 3.- Semiconductor detector electronics system and data readout.

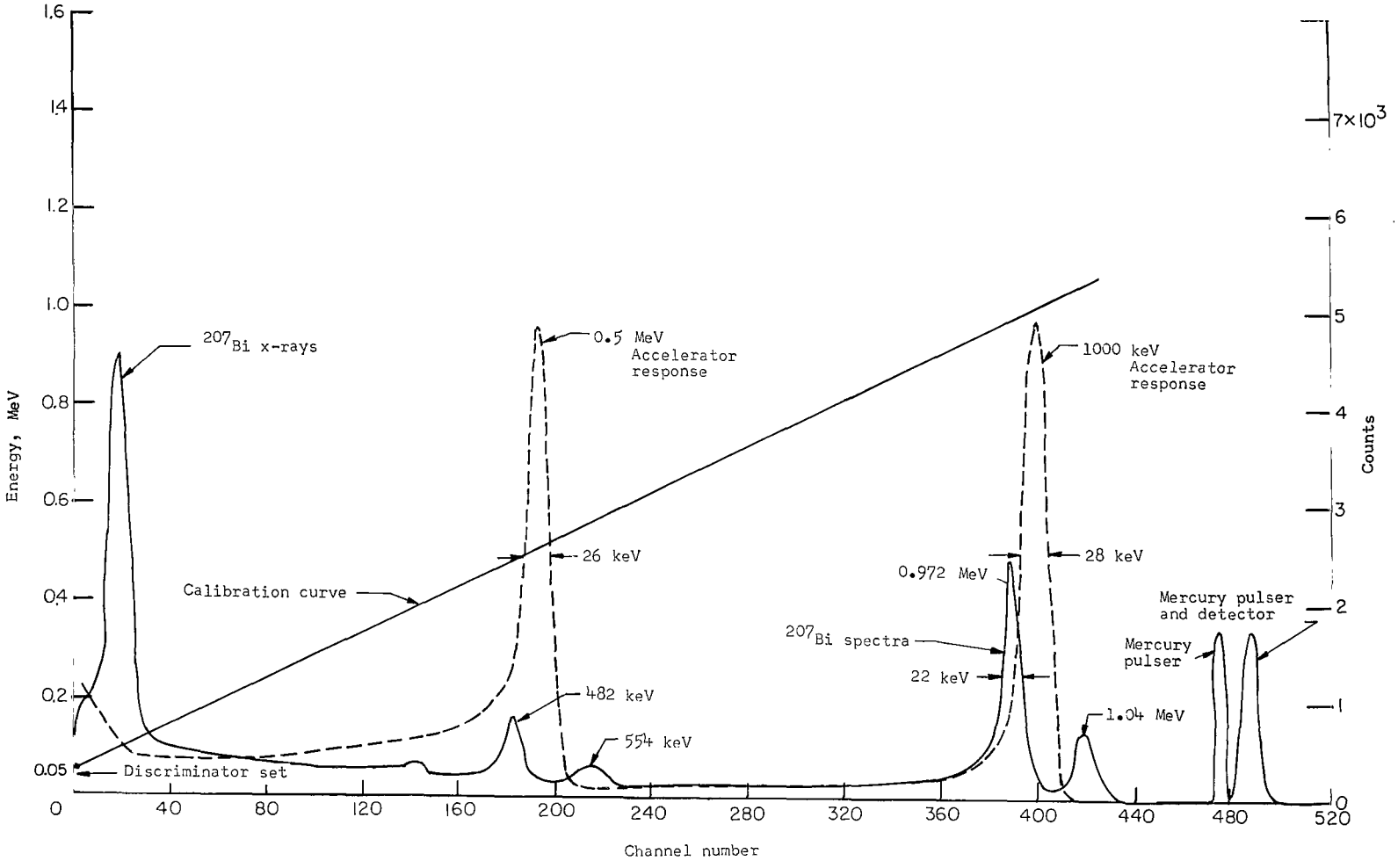

Figure 4.- Typical curves showing semiconductor detector response to ^{207}Bi, accelerator electron beam energy spread after passing through aluminum foil and electron energy calibration.

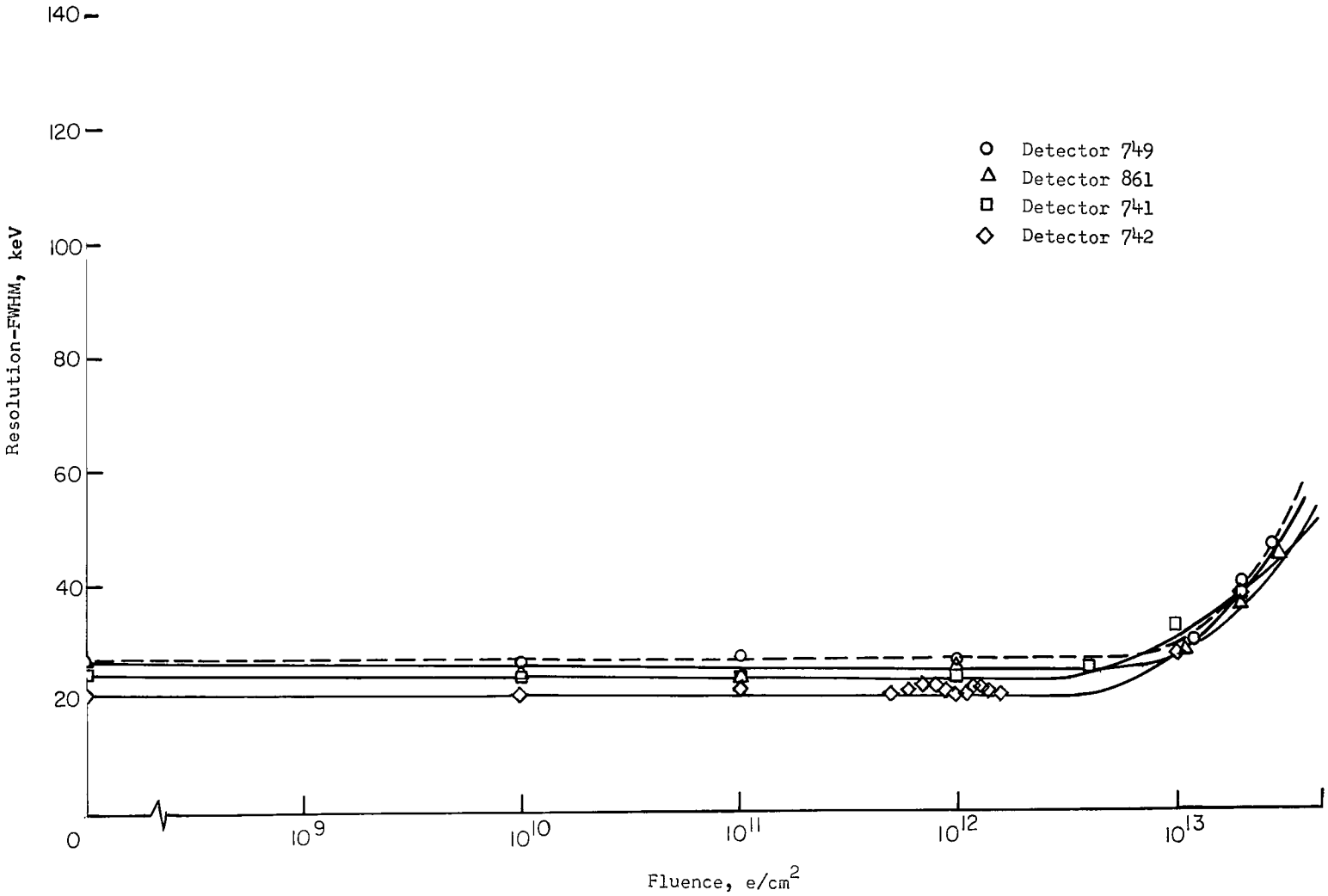

Figure 5.- Response changes in resolution of detectors irradiated with 0.5 MeV electrons.

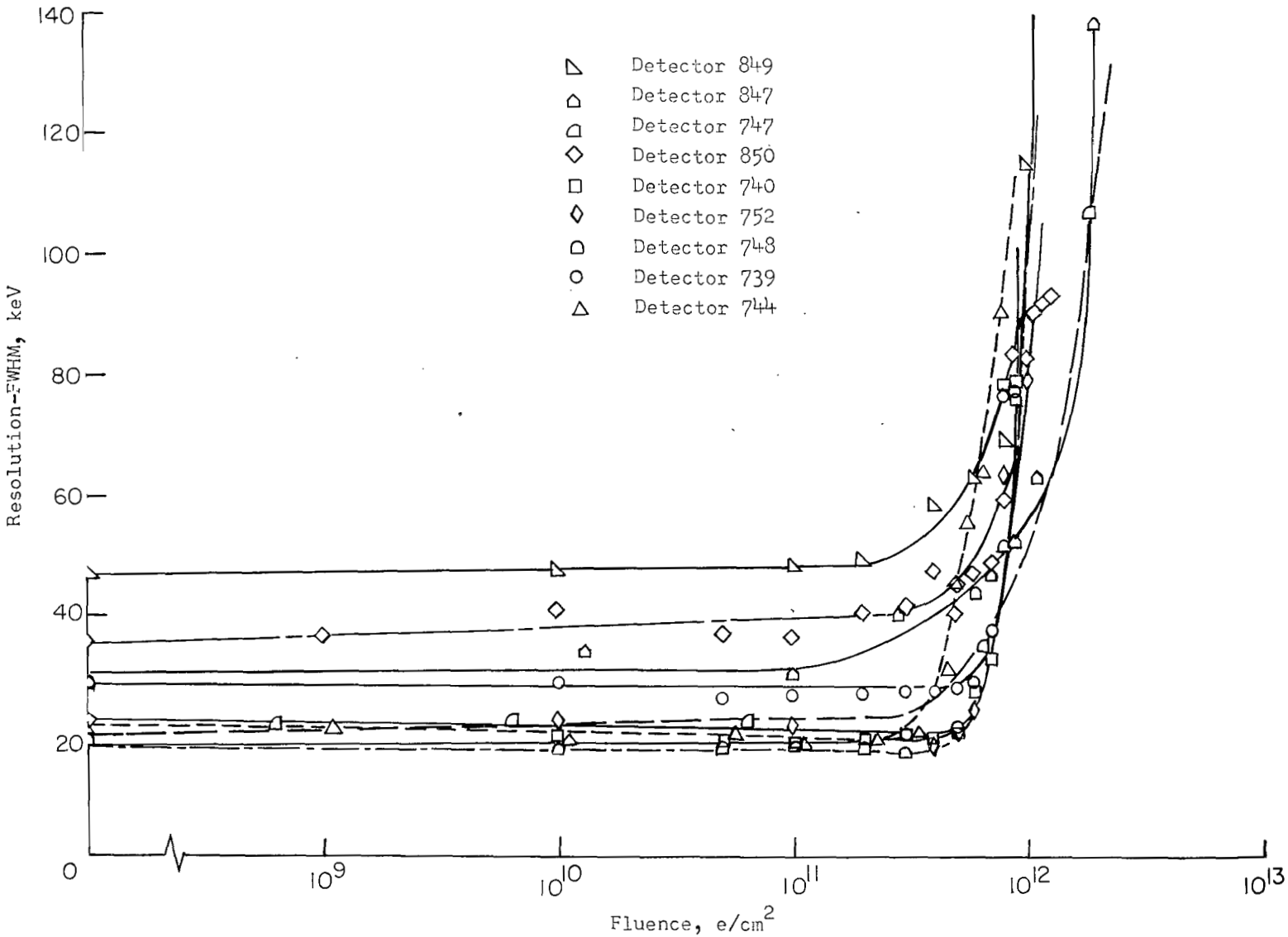

Figure 6.- Response changes in resolution of detectors irradiated with 1 MeV electrons.

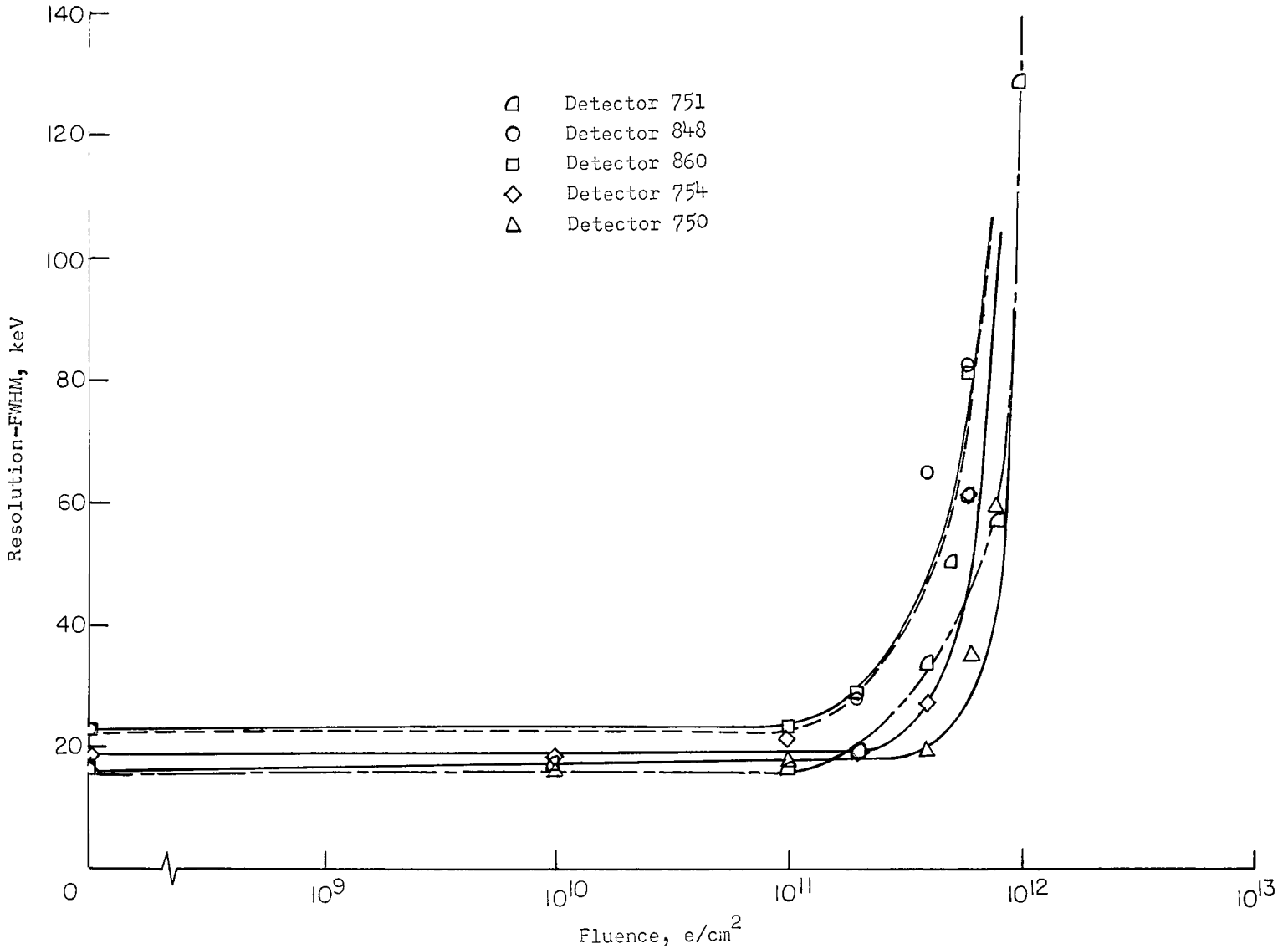

Figure 7.- Response changes in resolution of detectors irradiated with 2 MeV electrons.

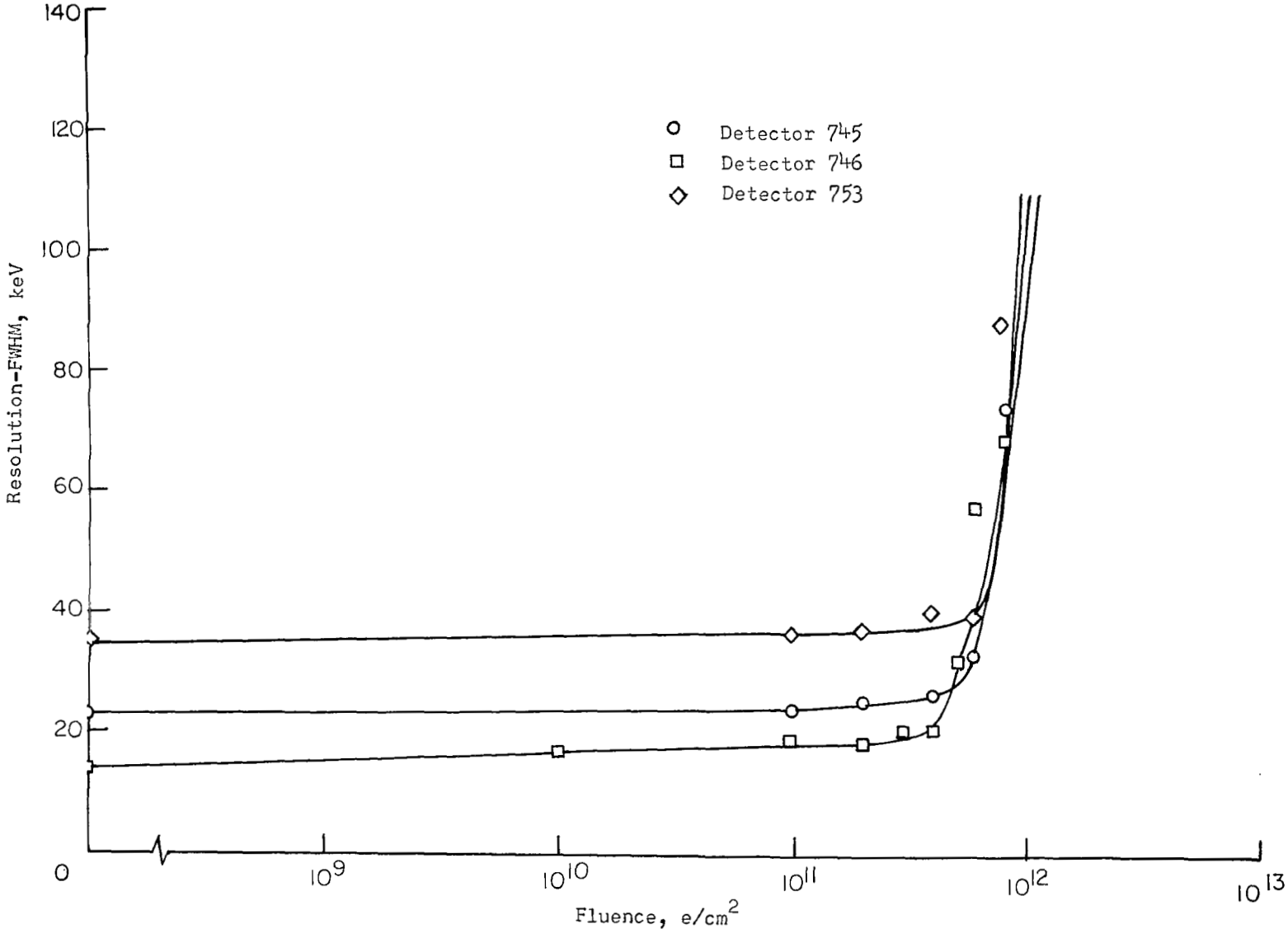

Figure 8.- Response changes in resolution of detectors irradiated with 3 MeV electrons.

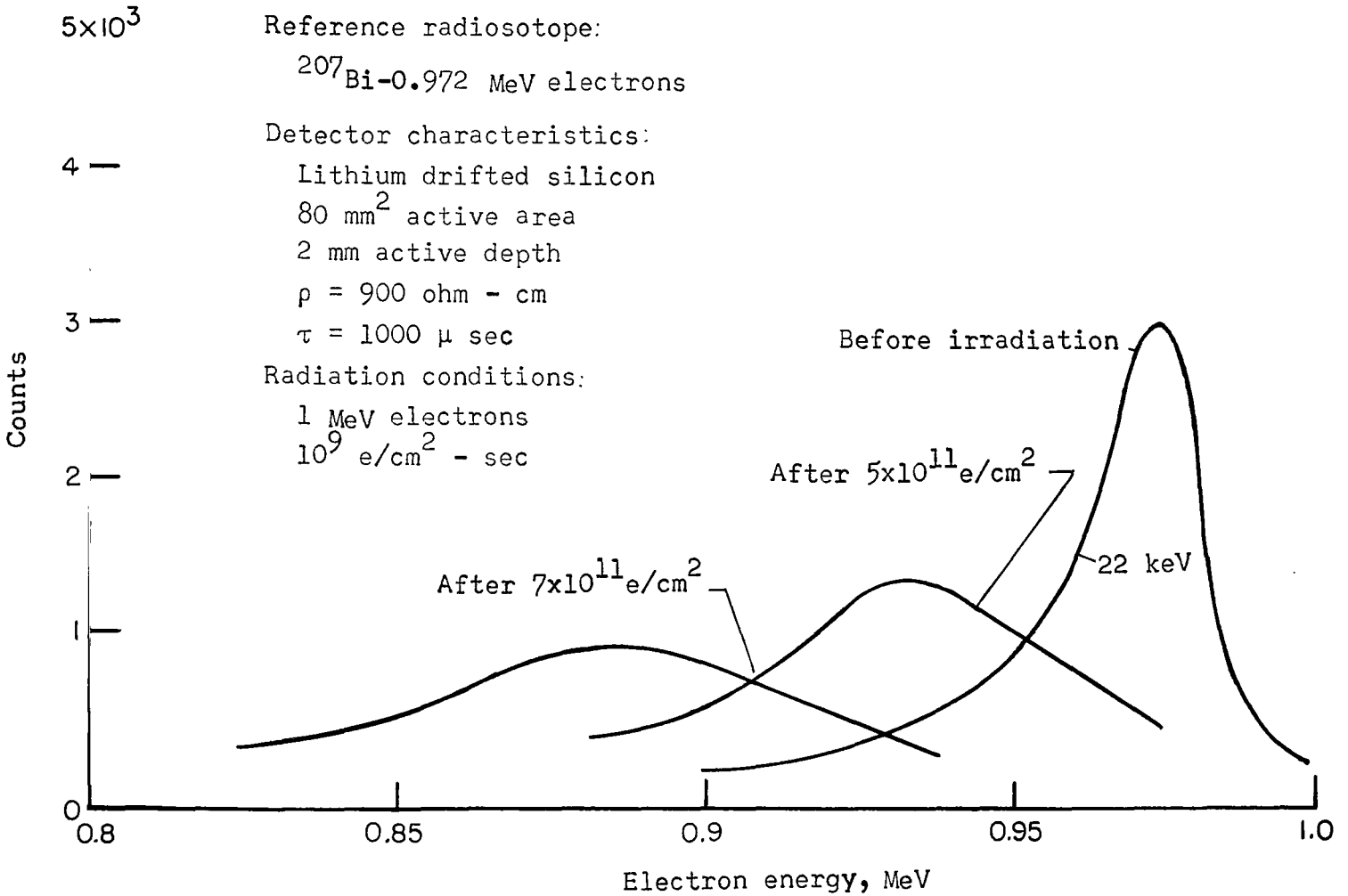

Figure 9.- Changes in the resolution of an irradiated semiconductor detector at different stages of irradiation.

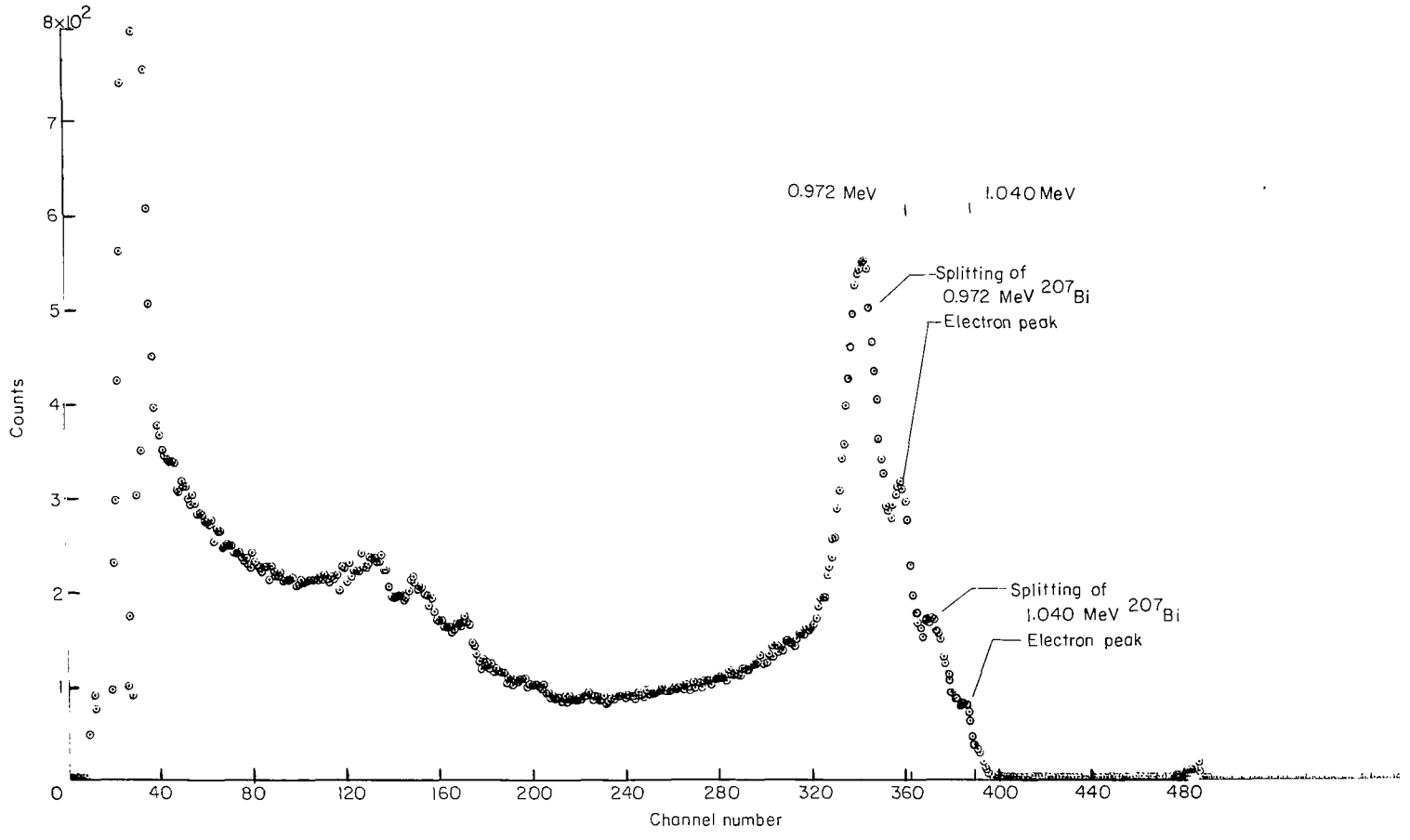

Figure 10.- Typical detector response curve showing multiple peaking of ^{207}Bi spectra peaks after electron irradiation of 0.5×10^{12} to 0.7×10^{12} e/cm2.

NATIONAL AERONAUTICS AND SPACE ADMINISTRATION
WASHINGTON, D. C. 20546

OFFICIAL BUSINESS

FIRST CLASS MAIL

POSTAGE AND FEES PAI
NATIONAL AERONAUTICS
SPACE ADMINISTRATIOI

POSTMASTER: If Undeliverable (Section
Postal Manual) Do Not R

"The aeronautical and space activities of the United States shall be conducted so as to contribute . . . to the expansion of human knowledge of phenomena in the atmosphere and space. The Administration shall provide for the widest practicable and appropriate dissemination of information concerning its activities and the results thereof."

—NATIONAL AERONAUTICS AND SPACE ACT OF 1958

NASA SCIENTIFIC AND TECHNICAL PUBLICATIONS

TECHNICAL REPORTS: Scientific and technical information considered important, complete, and a lasting contribution to existing knowledge.

TECHNICAL NOTES: Information less broad in scope but nevertheless of importance as a contribution to existing knowledge.

TECHNICAL MEMORANDUMS: Information receiving limited distribution because of preliminary data, security classification, or other reasons.

CONTRACTOR REPORTS: Scientific and technical information generated under a NASA contract or grant and considered an important contribution to existing knowledge.

TECHNICAL TRANSLATIONS: Information published in a foreign language considered to merit NASA distribution in English.

SPECIAL PUBLICATIONS: Information derived from or of value to NASA activities. Publications include conference proceedings, monographs, data compilations, handbooks, sourcebooks, and special bibliographies.

TECHNOLOGY UTILIZATION PUBLICATIONS: Information on technology used by NASA that may be of particular interest in commercial and other non-aerospace applications. Publications include Tech Briefs, Technology Utilization Reports and Notes, and Technology Surveys.

Details on the availability of these publications may be obtained from:

SCIENTIFIC AND TECHNICAL INFORMATION DIVISION

NATIONAL AERONAUTICS AND SPACE ADMINISTRATION

Washington, D.C. 20546